Journal of Marine Research, 55, 483–505, 1997

On the eddy transfer of tracers: Advective or diffusive?

by Mei-Man Lee[1], David P. Marshall[2] and Richard G. Williams[3]

ABSTRACT

Geostrophic eddies have traditionally been viewed within oceanography as diffusing water masses and tracers in a down-gradient manner. However, eddies also have an advective role that may lead to an up-gradient transfer of tracers, as has been recognized in atmospheric tracer studies and recent eddy parameterizations developed for the ocean. Eddies provide an advective transfer or "bolus" velocity through the secondary circulation formed by the slumping of density surfaces in baroclinic instability.

Here we use an eddy-resolving isopycnal ocean model to investigate the meridional transfer across a zonal jet. The jet undergoes baroclinic instability, forming a vibrant eddy field and inducing a meridional bolus velocity. The bolus velocity is found to be correlated with gradients of potential vorticity rather than thickness.

A transient tracer is released with high and low values at the southern and northern boundaries respectively. Over the first few years, the tracer spreads diffusively in a down-gradient manner. The implied eddy diffusivity of the passive tracer is found to be reassuringly similar to that of the dynamic tracer, potential vorticity. On the decadal time scale, however, the eddy-induced advection dominates and leads to a poleward spreading of tracer in the upper layer, and equatorward spreading of tracer in the lower layer. This eddy-induced advection is likely to be important in controlling the water-mass distribution wherever the time-mean meridional flow is weak. Observationally, the transport velocity is difficult to measure directly, but we argue might be inferred from the spreading of transient tracers, such as CFCs, before they reach a statistically-steady state.

1. Introduction

The large-scale distributions of temperature, salt, and other tracers, have provided valuable insights into the spreading of water masses through the ocean. A major advantage of focussing on a tracer field, rather than direct velocity measurements, is that the tracer field measures the time-integrated response of a body of water, even to a rapidly fluctuating velocity signal with a relatively modest background mean. The spreading of tracers can be achieved through the action of a time-mean circulation and a time-varying circulation.

Traditionally, the time-varying circulation has been viewed as providing a down-gradient diffusive transfer of water-mass properties. However recent work by Danabasoglu

1. Southampton Oceanography Centre, Empress Dock, Southampton, SO14 3ZH, United Kingdom.
2. Department of Meteorology, University of Reading, P.O. Box 243, Reading, RG6 6BB, United Kingdom.
3. Oceanography Laboratories, University of Liverpool, P.O. Box 147, Liverpool, L69 3BX, United Kingdom.

et al. (1994), Gent *et al.* (1995), and others, has highlighted how the time-varying circulation can also lead to a net eddy-induced advection of water masses. This eddy-induced advection may be particularly important in transporting water masses whenever the time-mean flow is weak: in dispersing ventilated water from regions of open ocean deep convection, in the meridional spreading of Antarctic Intermediate Water, North Atlantic Deep Water and Antarctic Bottom Water across zonal fronts in the Southern Ocean, and the poleward spreading of Mediterranean Water along the eastern coastline of Europe.

In the atmospheric community, the importance of eddy-induced transports is widely accepted following the seminal work of Andrews and McIntyre (1976), and Plumb and Mahlman (1987) in introducing the "residual" and "effective transport" circulations respectively—see Andrews *et al.* (1987) for an excellent review. For example, the Eulerian time-mean flow shows a poleward transport in the tropics in the Hadley cell, and an equatorward transport at middle latitudes in the Ferrel cell. However, when the mean and eddy transports are combined into a residual or effective transport circulation, then the Ferrel cell disappears and the Hadley cell extends to higher latitudes in the troposphere. A single circulation then extends from the low-latitude summer hemisphere to the high-latitude winter hemisphere in the stratosphere (Plumb and Mahlman, 1987).

In the oceanographic community, the eddy-induced advection has been incorporated into the eddy parameterization scheme of Gent and McWilliams (1990) and extensions by McDougall and McIntosh (1996), Treguier *et al.* (1997) and Visbeck *et al.* (1997).

In this study, our objectives are to:

(i) Diagnose the eddy-induced advection within an idealized, but eddy-resolving ocean model, and examine its relation to mean gradients of thickness and potential vorticity.

(ii) Examine the contrasting roles of the eddy-induced advection and diffusion for a passive tracer, and examine whether this advection is sufficiently strong to overcome diffusion, leading to up-gradient transfer.

(iii) Discuss how the eddy-induced advection might be identified within observational programs, such as WOCE, using hydrography, tracers or floats.

In Section 2, we review the concept of the eddy-induced bolus velocity and estimate, through a scale analysis, the time-scales over which the diffusive and advective roles of eddies are likely to be dominant. In Section 3, we introduce our eddy-resolving model which consists of a baroclinically-unstable jet maintained by buoyancy forcing, and diagnose the eddy-induced advection. In Section 4, we examine competing eddy closure hypotheses based on thickness and potential vorticity. In Section 5, we release a transient tracer into our model to examine the advective and diffusive transfers and, in Section 6, we discuss the problem of diagnosing the eddy-induced advection from these tracer fields. Finally, in Section 7, the implications of our results for observational and modeling programs are discussed.

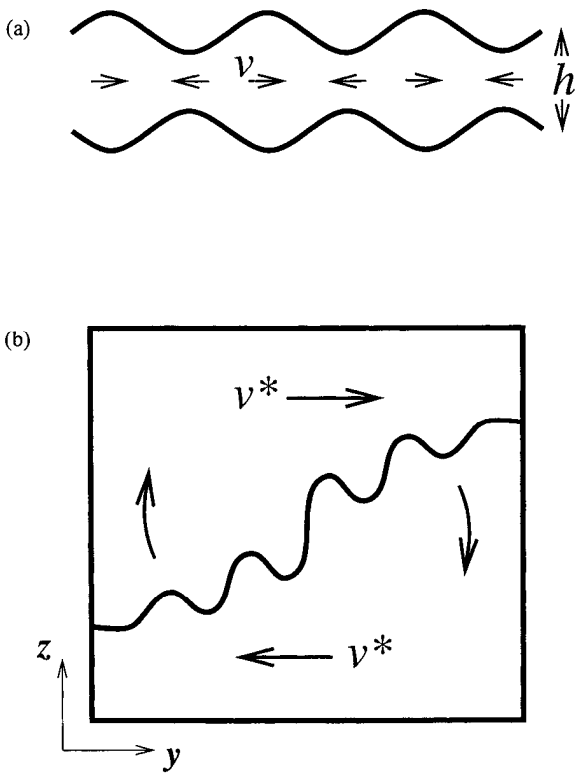

Figure 1. Schematic sections illustrating: (a) The time-averaged meridional volume flux in an undulating layer, $\overline{hv} = \bar{h}\bar{v} + \overline{h'v'}$, depends on advection by the time-mean meridional velocity $\bar{v}$, and the time-averaged correlation of the temporal deviations in velocity v' and layer thickness h'. (b) The slumping of isopycnals in baroclinic instability induces a secondary circulation in which the bolus velocity, $v^* = \overline{h'v'}/\bar{h}$, is poleward in the upper layer, and equatorward in the lower layer.

2. Theoretical background

Here, the role of eddies in driving a transport is reviewed and we discuss the importance of the diffusive and advective roles of eddies in transferring tracers.

a. Transport of water masses. The meridional transport of a water mass within an isopycnal layer is

$$V = hv,$$

where h is the thickness of the water-mass layer and v is its meridional velocity. Splitting the terms into time-mean and time-varying components, $h = \bar{h} + h'(t)$, $v = \bar{v} + v'(t)$, the time-mean transport is

$$\bar{V} = \bar{h}\bar{v} + \overline{h'v'}. \tag{1}$$

This total transport consists of the transport from the time-mean velocity, $\bar{h}\bar{v}$, and an addi- tional eddy-induced transport, $\overline{h'v'}$. The eddy-induced transport relies on an eddy correlation between layer thickness and velocity and is nonzero when a greater volume of water mass moves meridionally in one direction than returns in the opposite direction, as sketched in Figure 1a.

The time-mean transport can be rewritten as a "transport velocity" after dividing by the mean layer thickness,

$$(\bar{v} + v^*) = \bar{v} + \frac{\overline{h'v'}}{\bar{h}}. \tag{2}$$

In a limit of small-amplitude perturbations, this transport velocity is equivalent to the residual velocity derived in a transformed Eulerian-mean formulation (McIntosh and McDougall, 1996).

The eddy-induced velocity in (2) is

$$v^* = \frac{1}{\bar{h}} \overline{h'v'}, \tag{3}$$

and will henceforth be referred to as the "bolus velocity" following Rhines (1982) and McDougall (1991). The bolus velocity is particularly large in regions of baroclinic instability, where it represents the isopycnal component of the secondary circulation induced by the flattening of isopycnals (Fig. 1b). The bolus velocity is equivalent to the Stokes drift correction to the background flow for linear, steady waves,[4] see discussions by Plumb (1979) and Middleton and Loder (1989).

4. Consider the action of a linear, small amplitude, steady wave field with no background flow. For simplicity, assume that the oscillations in velocity are one-dimensional and given by

$$v'(y, t) = v_0 \sin(ky - \omega t).$$

Even though the Eulerian-mean velocity is zero, fluid parcels experience a net Stokes drift described by the velocity

$$v_{Stokes} \approx \frac{v_0^2 k}{2\omega}.$$

For a single layer of thickness $h = h_0 + h'$, the linearized continuity equation becomes

$$\frac{\partial h'}{\partial t} + h_0 \frac{\partial v'}{\partial y} \approx 0.$$

Substituting for v' gives a thickness perturbation varying as

$$h'(y, t) \approx \frac{h_0 v_0 k}{\omega} \sin(ky - \omega t),$$

which is in phase with the oscillating velocity v', precisely as sketched in Figure 1a. Thus, the bolus velocity is given by

$$v^* = \frac{1}{\bar{h}} \overline{h'v'} \approx \frac{v_0^2 k}{2\omega},$$

equivalent to the classical Stokes drift for linear, steady waves.

b. The evolution of a tracer field. The evolution of a tracer field depends on both advective and diffusive transfers. The importance of each process varies according to the controlling space and time scales.

To understand this contrasting processes, consider how a patch of dye spreads from a localized source using the time and zonal-mean tracer equation derived by Gent *et al.* (1995):

$$\frac{\partial \overline{C}}{\partial t} + (\bar{v} + v^*)\frac{\partial \overline{C}}{\partial y} = -\frac{1}{\bar{h}}\frac{\partial}{\partial y}\overline{(hv)'C'} \tag{4}$$

(a derivation and simplifying assumptions are given in the Appendix). The tracer field therefore evolves through advection by the transport velocity $(\bar{v} + v^*)$, and a term which is assumed to act in a diffusive manner,

$$-\frac{1}{\bar{h}}\frac{\partial}{\partial y}\overline{(hv)'C'} = \frac{1}{\bar{h}}\frac{\partial}{\partial y}\left(\bar{h}\kappa_c\frac{\partial \overline{C}}{\partial y}\right), \tag{5}$$

where κ_c is a tracer diffusivity. In Section 5c, we compare estimates of κ_c, diagnosed from a passive tracer in our model, with estimates of an independent diffusivity, κ_Q, diagnosed from the potential vorticity field. We find a close similarity between κ_c and κ_Q, supporting the overall validity of (5).

If the meridional spreading of tracer is controlled by *advection,* then (4) reduces to

$$\frac{\partial \overline{C}}{\partial t} \simeq -(\bar{v} + v^*)\frac{\partial \overline{C}}{\partial y}; \tag{6}$$

scale analysis suggests that the tracer spreads advectively over a spatial scale

$$L_{adv} \sim (\bar{v} + v^*)t,$$

where t is time.

Alternatively, if the spreading of tracer is controlled by *diffusion,* then (4) reduces to

$$\frac{\partial \overline{C}}{\partial t} \simeq \frac{1}{\bar{h}}\frac{\partial}{\partial y}\left(\bar{h}\kappa_c\frac{\partial \overline{C}}{\partial y}\right); \tag{7}$$

scale analysis suggests that the tracer spreads diffusively over a spatial scale

$$L_{dif} \sim (\kappa_c t)^{1/2}.$$

The ratio of these length scales is

$$\frac{L_{adv}}{L_{dif}} \sim \frac{(\bar{v} + v^*)}{\kappa_c^{1/2}}t^{1/2}. \tag{8}$$

Thus, for a nonzero $(\bar{v} + v^*)$ and κ_c, the initial spreading will be diffusive, since the ratio L_{adv}/L_{dif} is small. Over longer time scales, however, advection becomes important and

may eventually dominate over diffusion. For example, assuming $\kappa_c \sim 10^3\,\mathrm{m^2\,s^{-1}}$ and $(\bar{v} + v^*) \sim 10^{-3}\,\mathrm{m\,s^{-1}}$, suggests that advection and diffusion are comparable after ~30 years when the tracer has spread ~1000 km. However, if the transport velocity increases to $(\bar{v} + v^*) \sim 10^{-2}\,\mathrm{m\,s^{-1}}$, then advection and diffusion become comparable after ~3 years when the tracer has spread out to ~100 km.

3. Eddy-resolving experiment

An eddy-resolving experiment is now conducted to examine: (i) the role of eddies in advecting and diffusing tracers over a decadal time-scale, and (ii) whether the transport velocity can be identified and quantified from observations of a transient tracer.

Bolus velocities in the ocean can be generated through the slumping of density fronts in baroclinic instability. In a time-dependent slumping problem as studied by Gent *et al.* (1995), the bolus velocities are initially large, extracting potential energy from the front, but eventually reduce to zero as the slumping ceases. However, a statistically-steady bolus circulation can be maintained if the baroclinic front is itself maintained by buoyancy forcing (Marshall, 1997). This statistically-steady approach is followed here.

a. Model formulation. We use a free-surface primitive-equation model (Bleck and Smith, 1990) consisting of three isopycnal layers with σ = 27.5, 28.0, and 28.2. The domain consists of a zonally-periodic channel of meridional extent 1600 km and length 600 km (Fig. 2). A zonal jet is initialized by imposing meridional thickness gradients: the thickness of the upper layer varies from 1500 m at the south to 100 m at the north, the middle layer is a constant 500 m, and the thickness of the lower layer varies from 1500 m at the south to 2900 m at the north. The total depth of the ocean is a uniform 3500 m. The model does not include any forcing by a wind-stress, but instead buoyancy forcing is incorporated at the boundaries in order to maintain the zonal jet.

The prognostic equations for velocity and thickness of each layer are:

$$\frac{\partial u}{\partial t} - (f + \zeta)v + \frac{\partial B}{\partial x} = -D(u), \tag{9}$$

$$\frac{\partial v}{\partial t} + (f + \zeta)u + \frac{\partial B}{\partial y} = -D(v), \tag{10}$$

$$\frac{\partial h}{\partial t} + \frac{\partial}{\partial x}(hu) + \frac{\partial}{\partial y}(hv) = \mathscr{B}. \tag{11}$$

Here

$$B = \tfrac{1}{2}(u^2 + v^2) + M$$

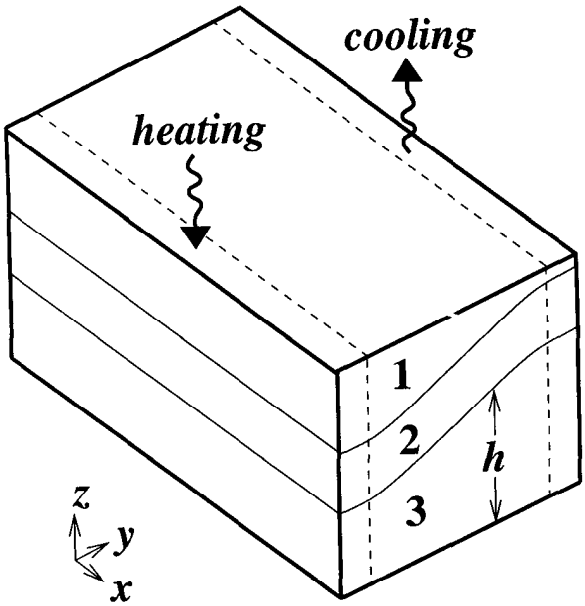

Figure 2. Schematic of the model domain consisting of a zonally-periodic channel with three density layers that are forced by heating and cooling in relaxation zones on the southern and northern boundaries.

is the Bernoulli potential,

$$\zeta = \frac{\partial v}{\partial x} - \frac{\partial u}{\partial y}$$

is the relative vorticity, h is the layer thickness, M is the Montgomery potential determined through hydrostatic balance, and $\mathscr{B}$ is the buoyancy forcing. The dissipation, D, includes a deformation-dependent friction in each layer (see Bleck and Boudra, 1981 for details) and a bottom friction with a spin-down time-scale of four months. No explicit diffusion is applied to the prognostic equation for h. The equations are solved on a C-grid with a model grid spacing of 10 km.

The model is integrated for an initial spin-up period of 12 years over which the model approaches a statistically-steady state, followed by a further integration for 18 years (labeled years 0 to 18) during which we inject passive tracers into the model. Time-stepping is through a leap-frog scheme with a time-step of 1200 s for the baroclinic modes, and 40 s for the free surface.

b. Buoyancy forcing and the statistically-steady circulation. Buoyancy forcing, $\mathscr{B}$, in our model is confined to two "relaxation" zones of width 200 km at the northern and southern boundaries (Fig. 2), where the layer thickness, h, is strongly relaxed toward its initial state,

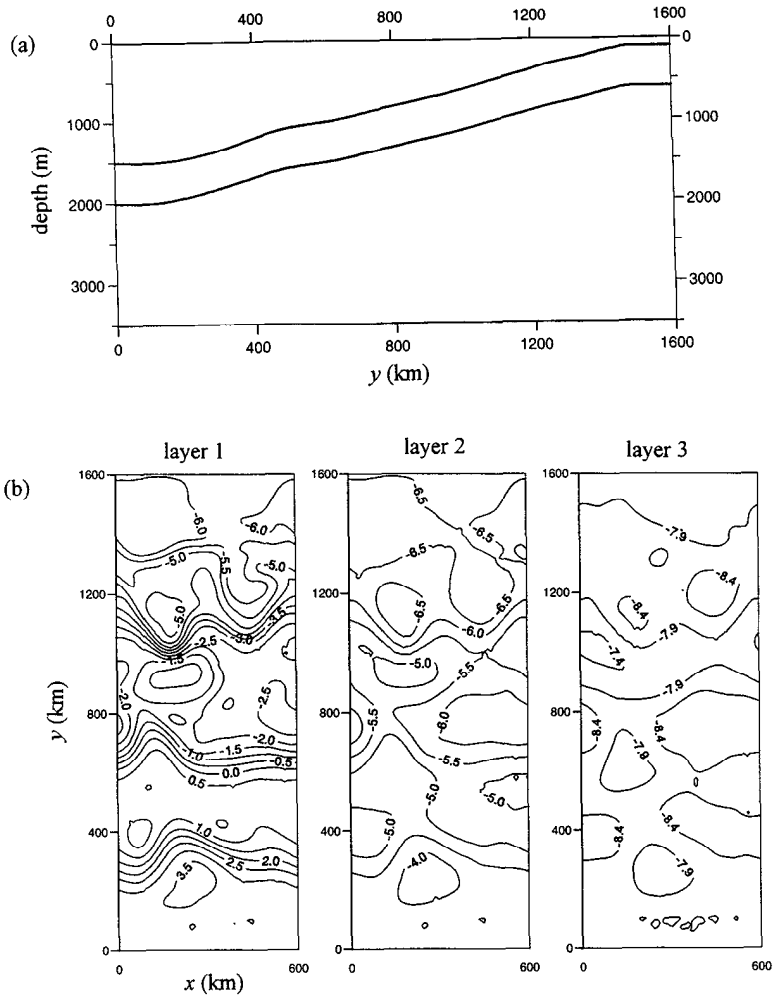

Figure 3. (a) Meridional section showing the depth of layer interfaces (m) at year 18; (b) Instantaneous geostrophic streamlines ($m^2\ s^{-2}$) for each layer at year 18 showing the eastwards jets in layer 1 and weaker recirculations in layers 2 and 3; (c) Time series of potential energy (10^2 J m^{-2}) and kinetic energy (10 J m^{-2}).

h_0:

$$\mathscr{B} = -\gamma(h - h_0). \tag{12}$$

The relaxation coefficient varies linearly from $\gamma = 0$ on the interior edge of the relaxation zone, to $10^{-3}\ s^{-1}$ at the solid boundaries. This buoyancy forcing maintains the meridional gradients in layer thickness (Fig. 3a). The strong gradients in layer thickness support, through the thermal-wind relation, an intense zonal jet. The jet has a zonal transport of

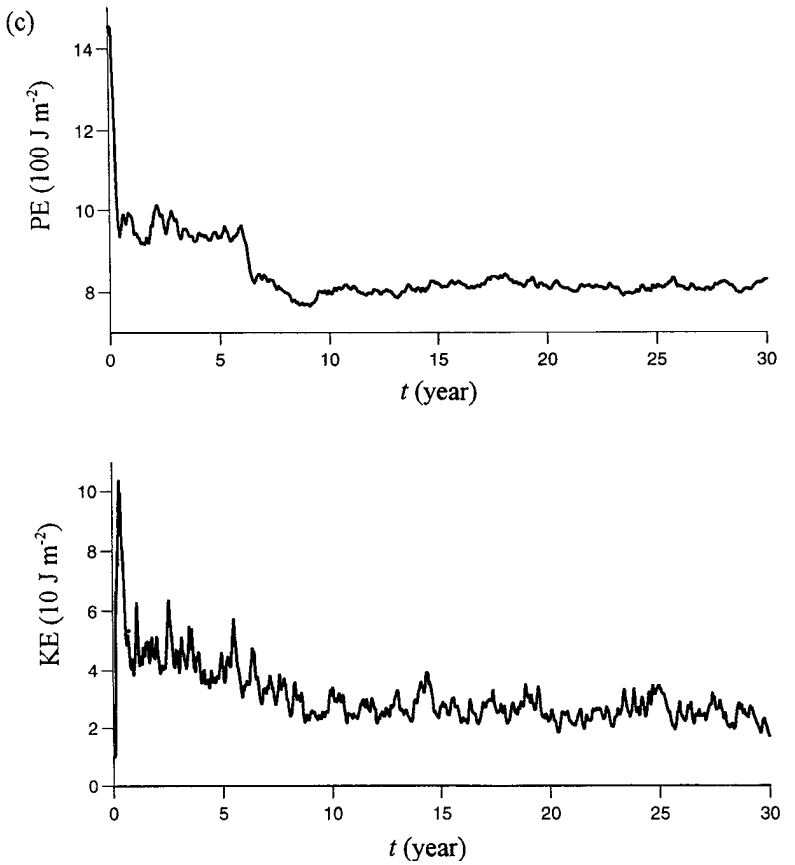

Figure 3. (Continued)

110 Sv (1 Sv $\equiv 10^6$ m^3 s^{-1}) with typical zonal velocities of 10 cm s^{-1} in layer 1 and -3 cm s^{-1} in layer 3.

The resulting zonal jet is baroclinically unstable and forms a vigorous geostrophic eddy field. Snapshots of the geostrophic streamlines within each layer at the end of year 18 are plotted in Figure 3b. The eddies have a typical horizontal scale of 50 km with horizontal velocities reaching 5 cm s^{-1}.

The eddies extract potential energy from the background mean state, which is compensated by an injection of potential energy by the buoyancy forcing. The potential energy and kinetic energy, integrated over the entire domain, are both close to a statistically-steady state after initial adjustments during the spin-up period, as confirmed in Figure 3c.

c. Meridional volume transports. The divergence of the meridional transport from the continuity equation is driven by the combination of the time-dependent slumping of the

layers and the buoyancy forcing, $\mathscr{B}$:

$$\frac{\partial \overline{h}}{\partial t} + \frac{\partial}{\partial y}(\overline{h}\overline{v} + \overline{h}v^*) = \overline{\mathscr{B}}. \tag{13}$$

As the integration is close to a statistically-steady state, the divergence of the meridional transport is large in the relaxation zones where there is buoyancy forcing. Even though the meridional transports in the interior are close to being nondivergent (and hence would not alter the local thickness), the transports are nonzero and thus important in transferring tracers (as seen later in Section 5).

The meridional transport consists of contributions from the time-mean and bolus velocities:

(i) The meridional stream function for the Eulerian-mean velocity, $\overline{v}$, reveals a series of weak overturning cells that change sign across the channel (Fig. 4a). The Eulerian-mean velocity, $\overline{v}$, is small since the geostrophic contribution integrates to zero in a zonal average:

$$\overline{h}\overline{v} = \frac{\overline{h}}{(f + \overline{\zeta})}\left\{\frac{\partial \overline{u}}{\partial t} - \overline{\zeta' v'} + \overline{D(u)}\right\}. \tag{14}$$

This remaining ageostrophic contribution is dominated by the Reynolds term ($\overline{\zeta' v'}$) in layers 1 and 2, with bottom friction also significant in layer 3.

(ii) In contrast, the stream function for the transport velocity, ($\overline{v} + v^*$), reveals a stronger, single overturning cell extending from the southern to northern relaxation zone (Fig. 4b). There is a strong poleward transport in layer 1, a weak poleward transport in layer 2 (even though there is uniform thickness), and a compensating equatorward transport in layer 3. The emergence of this single cell for the transport velocity is analogous to the near cancellation of both the tropospheric Ferrel Cell (Plumb and Mahlman, 1987) and the oceanic Deacon Cell (Danabasoglu *et al.*, 1994) when the eddy-induced transports are accounted for.

The implied meridional velocities in each layer can be inferred from the stream function shown in Figure 4. The time-mean meridional velocity is the order of 0.1 cm s^{-1} (Fig. 5a), whereas the eddy-induced transport corresponds to a bolus velocity of typically +0.15 cm s^{-1} in layer 1 and −0.05 cm s^{-1} in layer 3 (Fig. 5b). In layer 1, v^* is largest to the north where layer thickness is small. The lower value of v^* in layer 3 is a consequence of the larger layer thickness.

4. Parameterizations of the bolus velocity

We now diagnose eddy transfer coefficients based on closure hypotheses for thickness and potential vorticity and examine their connection with the bolus velocity.

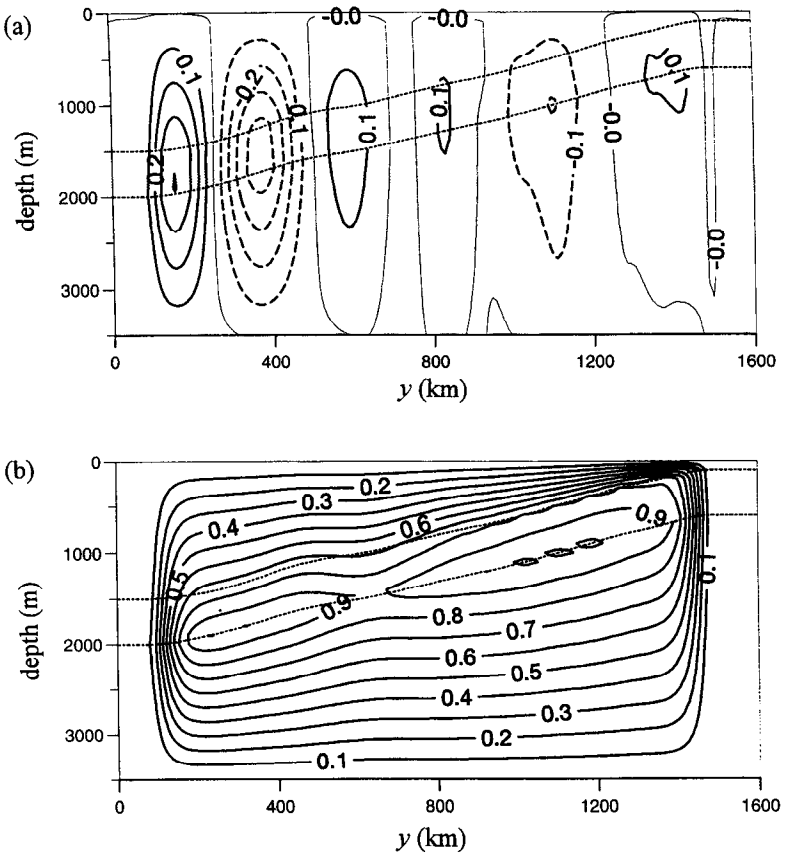

Figure 4. Meridional stream function $\psi = \int v dz$ ($m^2 s^{-1}$) evaluated from a time-average along isopycnals between years 12 and 18: (a) for the time-mean velocity $\bar{v}$ showing a series of overturning cells that reverse in direction between the southern and northern relaxation zones; (b) for the transport velocity $\bar{v} + v^*$ showing a single overturning cell extending between the relaxation zones. The short-dashed line shows the depth of the layer interfaces.

a. Eddy flux of thickness. Gent and McWilliams (1990) assume that the eddy flux of thickness is related to the mean gradient by an eddy closure hypothesis,

$$\overline{h'v'} = -\kappa_h \frac{\partial \bar{h}}{\partial y}, \tag{15}$$

where κ_h is defined as the eddy-transfer coefficient or diffusivity for layer thickness. Here, we diagnose κ_h using (15) from our eddy-resolving integrations. The implied κ_h reaches $\sim 1000\ m^2 s^{-1}$ in the upper and lower layers (Fig. 6a), but is ill-defined in layer 2 where $\partial \bar{h}/\partial y$ is close to zero. The similarity between κ_h in layers 1 and 3 follows from (15) since the meridional bolus transports are equal and opposite, $\bar{h}_1 v_1^* \simeq -\bar{h}_3 v_3^*$, and likewise the

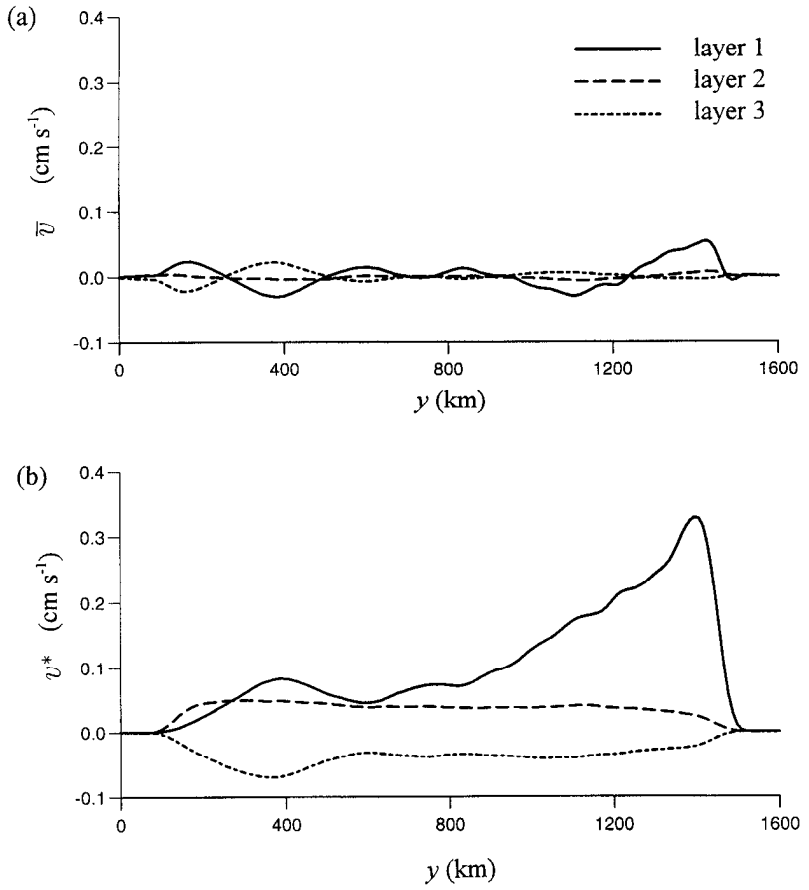

Figure 5. Zonal-mean meridional velocities (10^{-2} m s^{-1}) evaluated from a time-average between years 12 and 18: (a) time-mean Eulerian velocity $\overline{v}$, (b) bolus velocity $v^* = \overline{h'v'}/\overline{h}$.

meridional thickness gradients, $\partial\overline{h}_1/\partial y \simeq -\partial\overline{h}_3/\partial y$. This limited depth variation in κ_h is in contrast to the speculations of Gent *et al.* (1995) and Treguier *et al.* (1997), but may be a consequence of our idealized model geometry. κ_h is remarkably invariant within the jet, but decays to zero at the meridional walls where $v' \equiv 0$.

b. Eddy flux of potential vorticity. A shortcoming of the Gent and McWilliams eddy closure is that the layer thickness is not conserved by fluid parcels. We therefore examine an alternative eddy closure based on the potential vorticity, $Q = (f + \zeta)/h$, which is dynamically conserved,

$$\overline{Q'v'} = -\kappa_Q \frac{\partial \overline{Q}}{\partial y}, \tag{16}$$

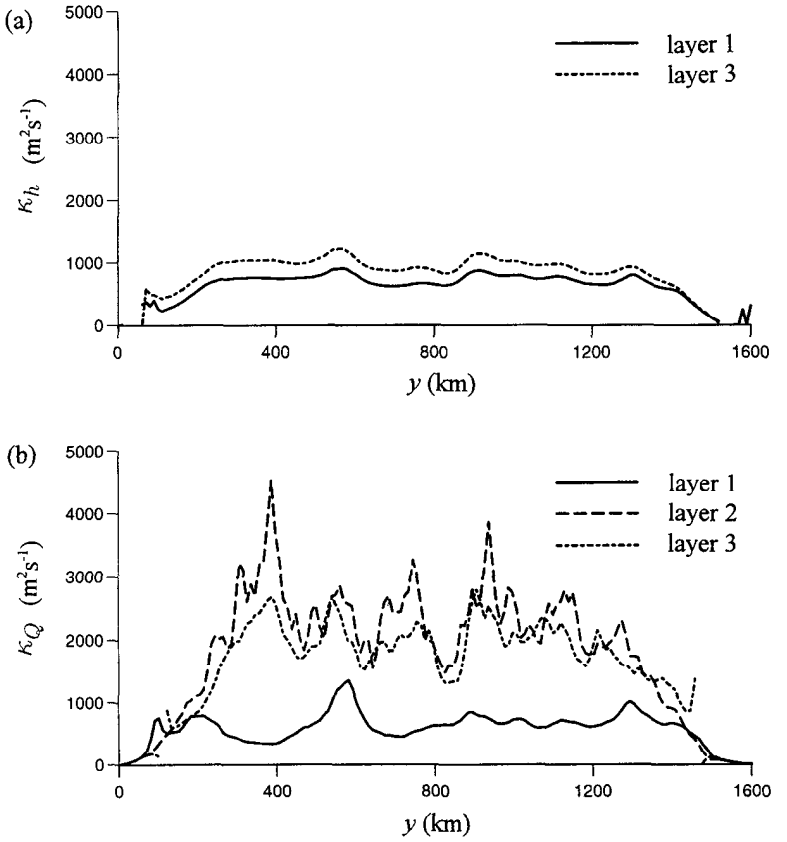

Figure 6. Diffusivity (m^2 s^{-1}) inferred from eddy fluxes and background gradients evaluated from a time-average between year 12 and 18: (a) for thickness, $\kappa_h = -\overline{h'v'}/(\partial\bar{h}/\partial y)$ for layers 1 and 3, (b) for potential vorticity, $\kappa_Q = -\overline{Q'v'}/(\partial\bar{Q}/\partial y)$ for each layer.

and use (16) to diagnose κ_Q, the implied eddy diffusivity for potential vorticity. In contrast to the previous calculation, κ_Q is well defined in all three layers. Encouragingly, $\overline{Q'v'}$ is directed down-gradient over the entire domain (apart from a few points adjacent to the relaxation zones) leading to positive values of κ_Q plotted in Figure 6b. In layer 1, κ_Q is similar in magnitude to κ_h; in layers 2 and 3, κ_Q is typically a factor of two larger ($\sim 2 \times 10^3$ m^2 s^{-1}). The diffusivity of this dynamic tracer, Q, is found to be very close to that of a passive tracer introduced in the next section (see Fig. 10).

The different magnitudes of κ_Q and κ_h may be understood by taking the ratio of (16) and (15) to obtain

$$\frac{\overline{Q'v'}}{\overline{h'v'}} = \frac{\kappa_Q \partial\bar{Q}/\partial y}{\kappa_h \partial\bar{h}/\partial y}. \tag{17}$$

On the large scale, $Q \approx f/\bar{h}$ and $\overline{Q'v'} \approx -f\overline{h'v'}/\bar{h}^2$, suggesting that (17) reduces to

$$\frac{\kappa_Q}{\kappa_h} \approx \left(1 - \frac{\beta \bar{h}}{f \partial \bar{h}/\partial y}\right)^{-1}. \tag{18}$$

Choosing values of $\bar{h} \sim 800$ m and $\partial \bar{h}/\partial y \sim -10^{-3}$ for the top layer, $\bar{h} \sim 2200$ m and $\partial \bar{h}/\partial y \sim 10^{-3}$ for the bottom layer, with $\beta \sim 2 \times 10^{-11}$ m^{-1} s^{-1} and $f \sim 10^{-4}$ s^{-1} gives ratios of $\kappa_Q/\kappa_h \sim 0.9$ and 1.8 for the top and bottom layers respectively, broadly consistent with our diagnosed values (Figs. 6a and 6b respectively).

c. Connections with the bolus velocity. Gent and McWilliams advocate parameterizing the bolus velocity in terms of the eddy closure for thickness,

$$v^*_{GM} = -\frac{\kappa_h}{\bar{h}} \frac{\partial \bar{h}}{\partial y}. \tag{19}$$

Alternatively, one can focus on the dynamically-conserved potential vorticity, $Q = (f + \zeta)/h$. Assuming small changes in background thickness, the linearized potential vorticity flux may be connected with the total eddy-induced velocity,

$$\overline{Q'v'} \simeq \frac{1}{\bar{h}} \overline{\zeta' v'} - \frac{(f + \bar{\zeta})}{\bar{h}^2} \overline{h'v'} = -\frac{(f + \bar{\zeta})}{\bar{h}} (v_{Reynolds} + v^*) \tag{20}$$

which incorporates both a time-mean velocity driven by Reynolds stresses and the bolus velocity. Treguier *et al.* (1997) argue that the Reynolds velocity is much smaller than the bolus velocity—this is supported by our experiments—and hence advocate parameterizing the bolus velocity in terms of the large-scale potential vorticity,

$$v^*_{THL} = \frac{\kappa_Q}{\bar{Q}} \frac{\partial \bar{Q}}{\partial y}. \tag{21}$$

Their justification is that Q is the conserved quantity rather than the layer thickness h.

In layers 1 and 3, our diagnosed v^* is broadly consistent with both parameterizations, (19) and (21) in being directed down the thickness gradient and up the potential vorticity gradient. However, in layer 2, there is zero thickness gradient due to our prescribed boundary conditions, but there is *still* a finite poleward bolus velocity. This result is consistent with the potential vorticity parameterization advocated by Treguier *et al.*, (21), whereas it is inconsistent with the thickness parameterization advocated by Gent and McWilliams, (1990). While this limit of zero thickness gradient is somewhat artificial, it does highlight how potential vorticity, rather than thickness, is the fundamental quantity.

Within an unforced layer of uniform potential vorticity, we would expect the eddy flux of potential vorticity to vanish and that the *total* eddy-induced velocity would likewise vanish

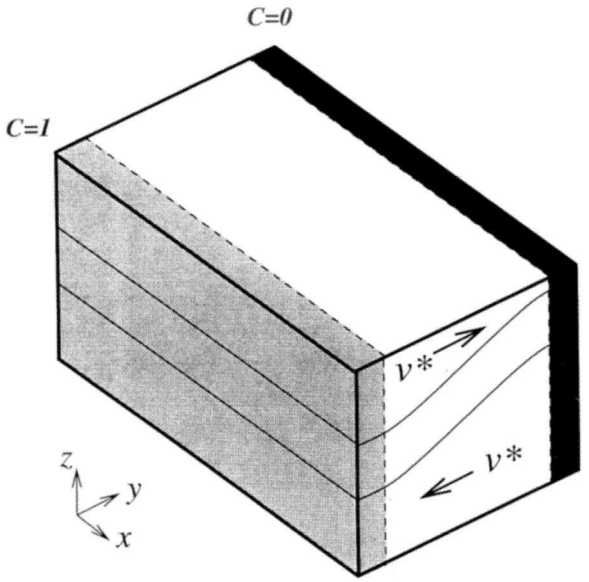

Figure 7. Schematic of tracer experiment showing high and low tracer released in the southern and northern relaxation zones. The tracer is transferred meridionally into the interior through diffusion and advection with the latter dominated by the bolus velocity, v^*.

by (20). Thus, the mean flow generated through Reynolds stresses, $v_{Reynolds}$, exactly cancels the eddy-induced bolus velocity, v^*.

5. Transient tracer experiment

A transient tracer is now released into our model to examine the competing advective and diffusive transfers by geostrophic eddies. Following the scale analysis in Section 2b, we expect diffusion to dominate the initial transfer of tracer, but eventually advection to become comparable or even dominate. After an initial dynamical spin-up, the tracer distribution is initialized with a passive, zonal front separating a value of 1 in the southern half of the domain and a value of 0 in the northern half.

The tracer equation is then integrated in an on-line manner with no explicit tracer diffusion

$$\frac{\partial C}{\partial t} + u\frac{\partial C}{\partial x} + v\frac{\partial C}{\partial y} = S, \tag{22}$$

where S represents prescribed tracer sources (and entrainment fluxes) within the relaxation zones. The tracer distribution is unforced in the interior, but strongly relaxed on a time scale of 10^3 s toward values of 1 and 0 within the 200 km-wide relaxation zones adjacent to the northern and southern boundaries (Fig. 7).

The tracer experiment is integrated for a further 18 years after the initial spin up of 12 years; the start of the tracer run is henceforth referred to as day 0.

a. Description of tracer evolution. The evolution of tracer is revealed in the instantaneous tracer maps shown in Figure 8 and in the zonally-averaged tracer sections shown in Figure 9.

After 5 days, the meandering zonal jet is seen to deform the initial front in the tracer field (Fig. 8a). The eddy activity is already starting to transfer high tracer poleward and low tracer equatorward in each of the layers; this is particularly evident over the eastern part of the jet in this snapshot.

After one year, the eddy transfer of tracer has been sufficiently strong to disperse the initial tracer front (Fig. 8b). There is a similar poleward decrease in tracer in each of the layers between the southern and northern relaxation zones. Superimposed on this background gradient, there are smaller-scale filaments of tracer resulting from the eddy activity. The rapid evolution of the tracer field away from the initial state is consistent with an initial diffusive control, as expected from the scale analysis in Section 2b. The zonally-averaged tracer section also shows the initial frontal signature at day 5 being smeared out to a nearly constant background gradient by year 1 (full and long dashed lines respectively in Fig. 9).

After 18 years, the large-scale tracer field has become strikingly asymmetric in layers 1 and 3, which is visible even with the deformation by the instantaneous eddy field (Fig. 8c). In layer 1, high tracer has been systematically advected poleward from the southern boundary and reaches the northern relaxation zone; in layer 3, low tracer has been instead advected equatorward from the northern boundary. There has been relatively little change in the tracer field in layer 2.

This advective character is also evident in the zonally-integrated sections shown in Figure 9: the meridional gradient in tracer becomes small over the interior, but is enhanced near the northern relaxation zone for layer 1; remains nearly uniform for layer 2; and is enhanced in the southern half of the domain for layer 3.

b. Interpretation of tracer evolution. The asymmetrical final tracer field is a consequence of the transport velocity and tracer boundary conditions applied on the northern and southern relaxation zones. The sign of the transport velocity selects which relaxation zone controls the interior tracer distribution (compare Figs. 4b and 8c). The transport velocity advects into the interior high tracer from the *southern* boundary for layer 1, and low tracer from the *northern* boundary for layer 3. For layer 2, we expect the weak poleward transport velocity to lead to a preferential spreading of high tracer from the southern boundary, but this signal is still unclear after 18 years.

In comparison, diffusion always attempts to transfer high tracer down-gradient from the source on the southern boundary. With regards the transfer of high tracer, advection and diffusion are acting in the same manner in layer 1, but are acting in *opposition* in layer 3. It

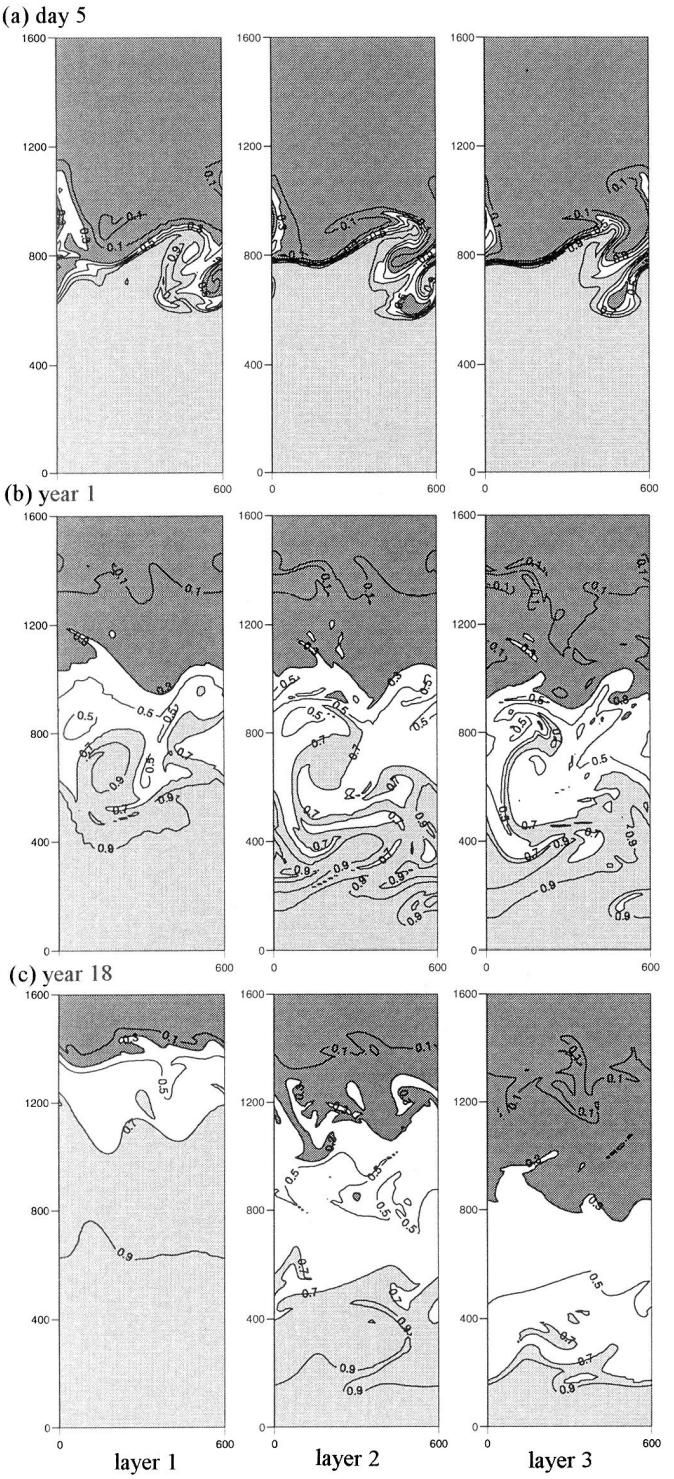

Figure 8. Time series of tracer fields for each layer at (a) day 5 of year 0, (b) year 1, and (c) year 18.

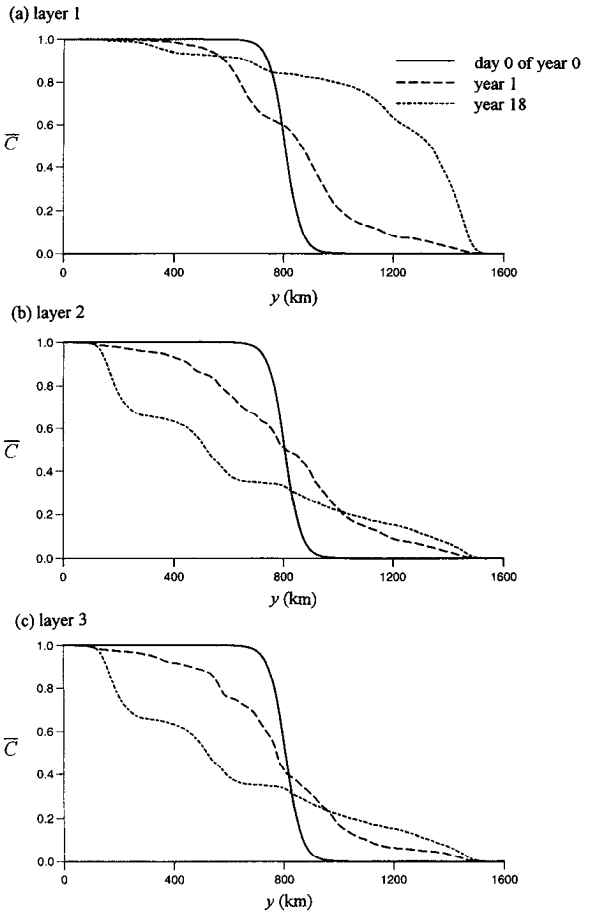

Figure 9. Meridional sections of zonally-averaged tracer for (a) layer 1, (b) layer 2 and (c) layer 3 at day 0 of year 0, year 1 and year 18.

is particularly striking how advection can be sufficiently strong to prevent the diffusive transfer of tracer, such as for the high tracer from its southern source in layer 3.

Thus, the interior tracer field takes up the inflow boundary conditions selected by the transport velocity, and with strong gradients being confined to an advective-diffusive boundary layer of width $\kappa_c/(\overline{v} + v^*)$ at the opposing boundary. The meridional advection of tracer contours is greater in layer 1, than in layer 3, due to the larger magnitude of the bolus velocity in the thinner layer (see Fig. 5).

This eventual dominance of advection over diffusion, leading even to an up-gradient transfer of tracer, is in accord with the scaling arguments in Section 2b; this result is also supported by additional integrations with different initial tracer conditions (not shown). It is particularly striking that the final tracer state bears no resemblance to that expected from advection by the time-mean flow (which is nearly zonal) and down-gradient diffusion.

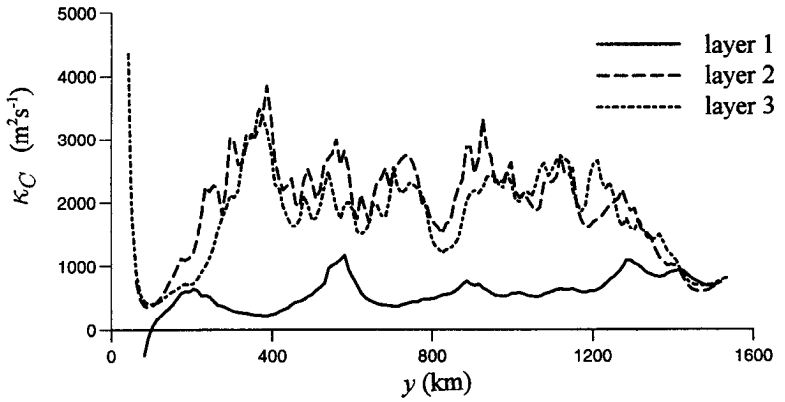

Figure 10. Tracer diffusivity (m^2 s^{-1}) inferred from eddy fluxes and background gradients evaluated from a time-average between year 12 and 18: $\kappa_c = -\overline{(hv)'C'}/(\bar{h}\partial\bar{C}/\partial y)$ for each layer. Note the similar distribution to κ_Q, shown in Figure 6b.

c. Diffusivity of tracer. While the tracer integration reveals the striking *advective* transfer of tracer by the eddies, there is also a diffusive transfer. Outside the relaxation zones, the time and zonally-averaged tracer equation (4) is again given by

$$\frac{\partial \bar{C}}{\partial t} + (\bar{v} + v^*)\frac{\partial \bar{C}}{\partial y} = -\frac{1}{\bar{h}}\frac{\partial}{\partial y}\overline{(hv)'C'}.$$

Following Gent *et al.* (1995), we suppose that the first term on the right-hand side acts in a diffusive manner, and defining a tracer diffusivity, κ_c, through the eddy closure hypothesis

$$\overline{(hv)'C'} = -\bar{h}\kappa_c\frac{\partial \bar{C}}{\partial y}. \tag{23}$$

Note that in this zonal channel, as $\bar{v}$ is relatively small, this eddy flux of tracer $\overline{(hv)'C'} \simeq \bar{h}\overline{v'C'}$, since $\overline{(hv)'} \equiv h'\bar{v} + \bar{h}v' \simeq \bar{h}v'$. The resulting diffusivity of tracer reaches 1000 m^2 s^{-1} in layer 1 and typically 2000 m^2 s^{-1} in layer 2 and 3 (Fig. 10). These diffusivities for the passive tracer are reassuringly similar to that inferred from the dynamic tracer, the potential vorticity, but not with that inferred from thickness; compare Figures 6a, 6b and 10. This result further supports the case that geostrophic eddies should be parameterized in terms of the dynamically conserved tracer, potential vorticity, rather than thickness.

6. Inferring the transport velocity from tracer observations

These eddy-resolving experiments demonstrate the importance of the transport velocity in controlling tracer, and hence water mass, distributions over large temporal and spatial scales. Given the importance of this process, we now discuss whether the transport

velocity, $(\bar{v} + v^*)$, can be deduced from the migration of tracer contours,

$$(\bar{v} + v^*) \approx -\frac{\partial \overline{C}/\partial t}{\partial \overline{C}/\partial y} + O\left(\frac{\kappa_c}{L}\right), \tag{24}$$

as one might attempt in an inverse calculation; here L is the horizontal scale of the tracer field.

Over the first few years when the horizontal scale is small, κ_c/L is large and diffusion dominates the migration of tracer contours. Thus, one cannot expect to measure the transport velocity from a tracer release experiment spanning only a few months or years.

However, one might succeed in observing and quantifying the transport velocity from the spreading of anthropogenic tracers invading the ocean over a decadal time-scale. For example, comparing the tracer fields in Figure 8 for years 1 and 18 reveals that the 0.5 contour migrates poleward by ~450 km in layer 1, and ~ −250 km in layer 3. These displacements imply a transport velocity $(\bar{v} + v^*) \sim +0.09$ cm s^{-1} in layer 1, and $(\bar{v} + v^*) \sim -0.05$ cm s^{-1} in layer 3. These tracer-inferred estimates of the transport velocity are similar to the independent, direct estimates of the bolus velocity shown in Figure 5b of typically $+0.15$ cm s^{-1} in layer 1 and -0.05 cm s^{-1} in layer 3. While the closeness of these estimates is perhaps fortuitous (given the bolus variation over the domain, neglect of diffusion and inherent errors in both estimates), their correct sign and similar order of magnitude does support the view that the transport velocity can be inferred from the migration of transient tracer contours.

Over longer time-scales, the inverse calculation becomes ill-posed since the tracer approaches a steady state and $\partial \overline{C}/\partial t \rightarrow 0$. At best, one can still infer the sign of the transport velocity by connecting the tracer to its source.

Consequently, there is a window over which the transport velocity might be deduced from the evolution of a transient tracer: this window lies between the initial diffusive transfer and the final statistically-steady state. Given sufficient sampling, such an approach could be applied to the spreading of anthropogenic tracers such as CFCs in the ocean.

7. Discussion

The ocean is an important part of the climate system through its global transfer of heat, freshwater and other tracers. Observational programs, such as WOCE, have attempted to identify the global water-mass and tracer distributions. These observational surveys allow the "spreading" of water masses away from their source regions to be identified following the core-analysis approach of Wüst (1935). However, it is difficult to define the mechanism by which tracers spread, as this depends on the action of both the time-mean and time-varying circulation. Given these problems in unambiguously identifying the circulation, one could choose to ignore tracer fields. However, we believe that tracers provide invaluable information about the Lagrangian movement or transport of water masses, which is not available from Eulerian measurements of the circulation.

In order to understand how water-mass distributions are controlled by the time-varying flow, we conduct tracer-release experiments in an eddy-resolving model of a zonal jet. The tracer spreads away from the sources with diffusion dominating over the first few years, but eventually advection dominates on the decadal time-scale. The advection can even lead to an up-gradient transfer of tracer, which is sufficiently strong to inhibit any down-gradient diffusive transfer. The eventual advective transfer is not achieved here by the time-mean geostrophic flow, but instead is due to a Stokes drift correction or bolus velocity from the time-varying flow together with a smaller contribution from the ageostrophic time-mean flow. It is striking that the final tracer distribution bears no resemblance to that expected from the advection by the time-mean flow and down-gradient diffusion.

This eddy-induced transport is likely to be important in transferring water masses whenever the time-mean circulation is weak. For example, in dispersing ventilated water masses away from open-ocean convection sites; in the meridional transfer of Antarctic Intermediate Water, North Atlantic Deep Water and Antarctic Bottom Water across the zonal fronts in the Southern Ocean; and the transfer of intermediate water masses, such as Mediterranean Water and Labrador Sea Water in the North Atlantic.

In interpreting observed water-mass distributions, it is therefore important to take proper account of the advection by the time-varying flow (McDougall, 1991). Inverse studies should obtain an *improved* fit to tracer distributions if they incorporate a parameterization of the eddy-induced transport. Indeed, for example, the ozone distribution in the stratosphere *cannot* be explained by only considering the effects of the photochemistry and time-mean circulation, but instead requires the eddy-induced transport to be included (see, for instance, James, 1994).

Our experiments broadly support the approach of Gent and McWilliams (1990) in attempting to parameterize eddy transports. However, our results suggest that an improved parameterization of the bolus velocity should be based on potential vorticity (as advocated by Treguier *et al.* 1997), rather than thickness, although in practise the modification is often likely to be subtle.

Ideally, one would prefer an independent measure of the bolus transport from observations. However, the bolus transport can only be resolved by accurate measurements of the time-mean correlation between velocity and layer thickness, which is extremely difficult to achieve over a wide domain and would require a dedicated sampling system.

A more attractive option is to measure the transport using a Lagrangian measure of the circulation, which naturally combines the contributions from the time-mean and bolus velocities. In principle, the displacement of floats are a possibility. However, preliminary modeling experiments (not shown here) suggest that the number of floats released in ocean experiments are unlikely to provide a reliable measure of the bolus transport due to sampling difficulties. Instead, we suggest that the spreading of transient tracers, such as CFCs, should be examined. The displacement of tracer contours over a decade should allow the total transport to be estimated. If the transport from the time-mean velocity is already known, then it should be possible to infer the bolus transport as a residual. There is

a window of opportunity to infer the total transport from the evolution of transient tracers, which lies between their initial diffusive transfer and their final, steady equilibrium.

Acknowledgments. We are grateful to the reviewers for their constructive comments. This study was supported by the EU MAST-2 program EUROFLOAT PL920057. MML is also grateful for support from EU MAST-2 program DYNAMO CT930060 and RGW for support from NERC UK WOCE Special Topic GST/02/813.

APPENDIX

Derivation of the time-mean tracer equation

Here, we present a brief derivation of the time-mean tracer equation, (4), following Gent *et al.* (1995) for adiabatic change and no explicit source of tracer.

Consider a layer of fluid of thickness h and velocity (u, v) in the (x, y) directions.

$$\frac{\partial h}{\partial t} + \frac{\partial}{\partial x}(hu) + \frac{\partial}{\partial y}(hv) = 0. \tag{A1}$$

Averaging (A1) both zonally, and in time over several eddy life-cycles, we find

$$\frac{\partial \overline{h}^{x,t}}{\partial t} + \frac{\partial}{\partial y}(\overline{h}^{x,t}\overline{v}^{x,t}) + \frac{\partial}{\partial y}(\overline{h'v'}^{x,t}) = 0. \tag{A2}$$

The superscripts are henceforth dropped for simplicity.

Similarly, the concentration of a tracer, C, evolves according to

$$\frac{\partial C}{\partial t} + u\frac{\partial C}{\partial x} + v\frac{\partial C}{\partial y} = 0. \tag{A3}$$

Combining (A3) with the continuity equation (A1), gives the evolution of the thickness-weighted tracer:

$$\frac{\partial}{\partial t}(hC) + \frac{\partial}{\partial x}(uhC) + \frac{\partial}{\partial y}(vhC) = 0. \tag{A4}$$

Now we take a zonal average and time-average over several eddy life-cycles to give

$$\frac{\partial}{\partial t}(\overline{h}\,\overline{C} + \overline{h'C'}) + \frac{\partial}{\partial y}[(\overline{h}\overline{v} + \overline{h'v'})\overline{C}] = -\frac{\partial}{\partial y}\overline{(hv)'C'}. \tag{A5}$$

In our model integrations, we find that the time-derivative of $\overline{h'C'}$ is negligible. Finally, using the continuity equation (A2), we obtain the time-mean tracer equation,

$$\frac{\partial \overline{C}}{\partial t} + (\overline{v} + v^*)\frac{\partial \overline{C}}{\partial y} \approx -\frac{1}{\overline{h}}\frac{\partial}{\partial y}\overline{(hv)'C'}, \tag{A6}$$

where $v^* = \overline{h'v'}/\overline{h}$ is the bolus velocity defined in (3).

REFERENCES

Andrews, D. G., J. R. Holton and C. B. Leovy. 1987. Middle Atmosphere Dynamics, Academic Press, New York, 489 pp.

Andrews, D. G. and M. E. McIntyre. 1976. Planetary waves in horizontal and vertical shear: The generalised Eliassen-Palm relation and the zonal mean acceleration. J. Atmos. Sci., *33,* 2031–2048.

Bleck, R. and D. Boudra. 1981. Wind-driven spin-up in eddy-resolving ocean models formulated in isopycnic and isobaric coordinates. J. Geophys. Res., *91,* 7611–7621.

Bleck, R. and L. T. Smith. 1990. A wind-driven isopycnic coordinate model of the North and Equatorial Atlantic Ocean. I. Model development and supporting experiments. J. Geophys. Res., *95,* 3273–3285.

Danabasoglu, G., J. C. McWilliams and P. R. Gent. 1994. The role of mesoscale tracer transports in the global ocean circulation. Science, *264,* 1123–1126.

Gent, P. R. and J. C. McWilliams. 1990. Isopycnal mixing in ocean circulation models. J. Phys. Oceanogr., *20,* 150–155.

Gent, P. R., J. Willebrand, T. J. McDougall and J. C. McWilliams. 1995. Parameterising eddy-induced tracer transports in ocean circulation models. J. Phys. Oceanogr., *25,* 463–474.

James, I. N. 1994. Introduction to Circulating Atmospheres, Cambridge University Press, Cambridge, 422 pp.

Marshall, D. P. 1997. Subduction of water masses in an eddying ocean. J. Mar. Res., *55,* 201–222.

McDougall, T. J. 1991. Parameterising mixing in inverse models. Dynamics of Oceanic Internal Gravity Waves, P. Muller and D. Henderson, eds., Proc. Sixth 'Aha Huliko'a Hawaiian Winter Workshop, University of Hawaii at Manoa, 355–386.

McDougall, T. J. and P. C. McIntosh. 1996. The temporal-residual-mean velocity: I. Derivation and the scalar conservation relations. J. Phys. Oceanogr., 26, 2653–2665.

McIntosh, P. C. and T. J. McDougall. 1996. Isopycnal averaging and the residual mean circulation. J. Phys. Oceanogr., *26,* 1655–1660.

Middleton and Loder. 1989. Skew fluxes in polarised wave fields. J. Phys. Oceanogr., *19,* 196–199.

Plumb, R. A. 1979. Eddy fluxes of conserved quantities by small-amplitude waves. J. Atmos. Sci., *36,* 1699–1704.

Plumb, R. A. and J. D. Mahlman. 1987. The zonally averaged transport characteristics of the GFDL General Circulation Model. J. Atmos., Sci., *44,* 298–327.

Rhines, P. B. 1982. Basic dynamics of the large-scale geostrophic circulation. Summer Study Program in Geophysical Fluid Dynamics, Woods Hole Oceanographic Institution, 1–47.

Treguier, A. M., I. M. Held and V. D. Larichev. 1997. On the parameterisation of quasi-geostrophic eddies in primitive equation ocean models. J. Phys. Oceanogr., *27,* 567–580.

Visbeck, M., J. Marshall, T. Haine and M. Spall. 1997. Specification of eddy transfer coefficients in coarse resolution ocean circulation models. J. Phys. Oceanogr., *27,* 381–402.

Wüst, G. 1935. Schichtung und Zirkulation des Atlantischen Ozeans. Die Stratosphäre. *in* Wissenschaftliche Ergebnisse der Deutschen Atlantischen Expedition auf dem Forschungs—und Vermessungsschiff "Meteor" 1925–1927, 6: 1st part, 2, 180 pp.

Received: *18 June, 1996;* revised: *10 December, 1996.*